Journal of Power Sources 195 (2010) 5429–5441

Contents lists available at ScienceDirect

Journal of Power Sources

journal homepage: www.elsevier.com/locate/jpowsour

Review

Structural and wetting properties of fuel cell components

Yu. M. Volfkovich*, V.E. Sosenkin, V.S. Bagotsky

A.N. Frumkin Institute of Electrochemistry and Physical Chemistry, Russian Academy of Sciences, Moscow, Russia

ARTICLE INFO

Article history:
Received 13 January 2010
Received in revised form 28 February 2010
Accepted 1 March 2010
Available online 6 March 2010

Keywords:
Structural properties
Wetting properties
Porous fuel cell components
Porosimetry
Hydrophobizing effect
Inversion of ionogenic groups

ABSTRACT

The operation of proton exchange membrane (PEMFC) and direct methanol fuel cells (DMFC) is connected with the flow of different gaseous and liquid components in the cell's membrane-electrode assembly (MEA). The structural and wetting properties of different components of the MEA influence the rate and direction of these flows and hence the fuel cell's efficiency.

For a better understanding of the mechanism of all processes influencing the fuel cell efficiency, for a mathematical modelling of these processes, and for a possibility of their optimization, a detailed knowledge of the geometrical structure and wetting properties of all MEA components is necessary.

This review describes the results of such investigations performed mainly by using the method of standard contact porosimetry (MSCP). This method gives the possibility to receive information on multicomponent porous and powdered materials hitherto not accessible, viz. their wetting and swelling properties, pore corrugation, and also isotherms of capillary pressure and bond energy. Measurements of MEA components by this method can be performed under exactly the same conditions (temperature, compression degree, contact with water, etc.) as those existing in real fuel cells.

© 2010 Elsevier B.V. All rights reserved.

Contents

* Corresponding author.
E-mail addresses: yuvolf40@mail.ru (Yu.M. Volfkovich), vbag@mail.ru (V.S. Bagotsky).

0378-7753/$ – see front matter © 2010 Elsevier B.V. All rights reserved.
doi:10.1016/j.jpowsour.2010.03.002

1. Introduction

The operation of a fuel cell involves the flow of different gaseous and liquid components in the membrane-electrode assembly (MEA). Reactants must be supplied from the outside to the catalytic layer with a rate depending on the cell's discharge current and the reaction products must be removed from this layer with an analogous rate. In low temperature fuel cells operating at temperatures below approx. 120 °C (PEMFC and DMFC) in which polymer ion conducting membranes are used as electrolyte, water is present in gaseous state as well as in liquid state. A part of the pores in these fuel cells mainly formed by metallic catalyst particles have hydrophilic properties and are easily wetted by liquid water. Another part of the pores formed by carbonaceous particles and by some additives having hydrophobic properties remain dry during fuel cell operation and thus can be used for the transport of gaseous reagents. The operational reliability and durability of this type of fuel cells depend on a proper water management connected with the choice of predetermined flow directions for vapor and liquid water in the MEA pore network [1,2].

For a better understanding of the mechanism of all processes influencing the fuel cell efficiency, for mathematical modelling of these processes, and for a possibility of their optimization, a detailed knowledge of the geometrical structure and of the wetting (hydrophobic–hydrophilic) properties of the all components of the MEA is necessary.

The geometric structure of porous materials can be characterized by porograms, viz. the integral pore size distribution function (PSDF) describing the distribution of pore volume vs. pore radii V, r, or the differential PSDF (dV/dr), r.

Using the equation:

$$S_{\text{pore}} = 2\int_0^r \left(\frac{1}{r}\right)\left(\frac{dV}{dr}\right)\, dr, \tag{1.1}$$

these functions allow calculating another important parameter of the porous structure – the distribution function of the pore's surface S vs. pore radii S, r.

The purpose of this review is to analyze in more detail the existing information on structural and wetting properties of the porous components of fuel cell and on attempts to correlate these properties with the efficiency of fuel cell operation.

2. Methods for investigation of porous materials

2.1. Methods for investigation of structural properties

The best-known method for investigating the porous structure of different materials is the method of mercury porosimetry MMP described in Ref. [3]. This method is based on intrusion of mercury into samples of the porous material under high pressure. When an external pressure P is applied, all pores with radii $r > r_{\min}$ become filled with mercury. The value of $r_{\min}$ corresponds to the condition that the mercury capillary pressure p^c in the pore is equal to the applied pressure P. The capillary pressure is determined by the thermodynamic Laplace equation:

$$p^c = 2\sigma\frac{\cos\theta}{r_{\min}}, \tag{2.1}$$

where σ is the excess surface energy or "surface tension" (for mercury $\sigma = 4.67\ \mu J\,cm^{-2}$), θ is the wetting angle of liquid mercury with the given material. Therefore, measuring the dependence of the mercury volume V_{Hg} introduced into the sample under the applied pressure P the integral distribution function, of pore volumes V_{pore} vs. capillary pressure (or when the value of θ is known, vs. pore radii) is found. This method provides the widest range of measurable pore radii (from 2 nm to 10^5 nm). The accuracy of this method is very high. For these reasons it is widely used for the investigation of the geometric structure of different porous materials. Devices for automated measurements by MMP with a direct recording of the results are available on the market.

At the same time this method has some serious drawbacks. It requires the application of high pressures (up to thousands bar). This can lead to deformation or even destruction of the samples and, thus, to distortion of porograms. For this reason MMP cannot be applied to investigate soft and frail materials. Also this method cannot be applied for investigation of metals that are amalgamated by mercury. These drawbacks of MMP prevent the use of this method for most components of fuel cells, such as:

(1) membranes, parts which are made of porous carbonaceous materials, and gas-diffusion layers which would be deformed under high pressure; or
(2) catalytic layers with metal catalysts (platinum a.o.) which would be partially amalgamated by mercury.

Several other methods for investigating the structure of porous materials are also known. Each of these methods has its own advantages and limitations. Small angle X-ray scattering [4] can be used only for pore radii from 2 to 50 nm and often leads to ambiguous results. Electronic spectroscopy is associated with difficulties in pretreatment of the samples and interpretation of the results. Centrifugal porosimetry [5], displacement of wetting liquids from the pore volume by gas pressure [6], and optical methods are practically useless for pore sizes below 10^3 nm. The method of capillary condensation [7] can be used only in the pore size range from 1 to 50 nm. Other methods that were used for the investigation of the porous structure of different materials are: hydraulic permeability [8,9], electron microscopy [10,11] atomic force microscopy [12].

2.2. Methods for investigation of wetting properties

The degree of hydrophobic properties for materials with a smooth surface can be characterized by the wetting angle of a water drop placed on this surface. However, this method cannot be used in porous materials for two reasons: (1) the surface roughness of these materials leads to a distortion of the wetting angle and (2) it reflects only the wetting properties of the external surface of the sample, but not those of inside pores.

In 1921 Washburn [13] proposed a method for determining the internal wetting angle of water in porous media. This method is based on measuring the rate of water rise in a suspended sample of

the porous material. It is not applicable for partially hydrophobic materials.

2.3. The method of standard contact porosimetry (MSCP)

Because of the shortcomings and limited possibilities of other methods for investigating the porous structure of fuel cell components, a new method for porosimetric measurements was developed in the 1980s at the A.N. Frumkin Institute of Electrochemistry of the Russian Academy of Sciences It is called the Method of Standard Contact Porosimetry (MSCP). This method was described in Refs. [14–17] and discussed more in detail in Refs. [18,19].

2.3.1. Principles of the method

The method is based on the laws of capillary equilibrium. If two (or more) porous bodies partially filled with a wetting liquid are in capillary equilibrium, the values of the liquid's capillary pressure p^c in these bodies are equal. In this method the amount of a wetting liquid in the test sample (V_t) is measured. Simultaneously the amount of the same wetting liquid is measured in a standard specimen of known porous structure (V_s). The liquids in both porous samples are kept in contact. After some time a thermodynamic equilibrium is established. The measurements are performed for different overall amounts of the liquid $V_0 = V_s + V_t$. During the experiment this overall amount is changed by gradual evaporation of the liquid.

These measurements allow to establish the distribution of pore volume vs. pore size of the test sample by comparing with the known PSDF of the standard sample. Fig. 1 shows how this can be done graphically for the case when wetting of both samples by the liquid is ideal ($\theta = 0^\circ$, $\cos\theta = 1$), curve 1 On the left side of this figure represents the experimental dependence of the volume V_s in the standard sample on the volume V_t in the test sample for different values of V_0. On the right side, the integral pore size distribution curves (pore volume as a function of $\log r$) are shown. Curve 2 is the known PSDF curve for the standard sample. For a certain total volume of liquid V_o', the volumes of liquid in both bodies V_s' and V_t' are represented by the coordinates of point C. This point corresponds to point D on curve 2 and to a certain value r' of the minimal radius of filled pores. In the case of capillary equilibrium (under the assumption made), the minimal radius of filled pores in the test sample will be the same. As in this sample the volume of liquid is represented by point B (the line is drawn at an angle of 45°), point E corresponds to a point on the pore size distribution curve for the test sample. Thus, changing the value of the total volume V_o of the liquid, the overall distribution curve 3 for the test sample can be determined.

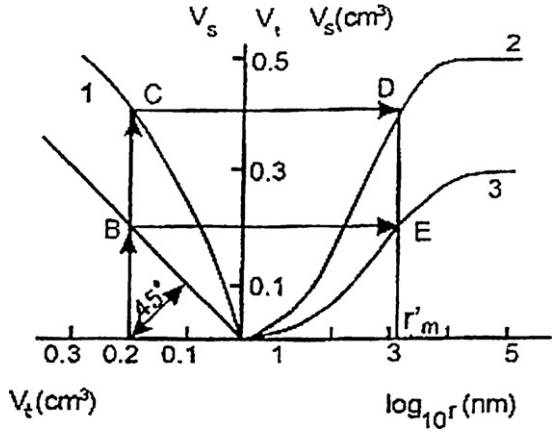

Fig. 1. Example for determining pore size distribution curves by MSCP: (1) dependence of V_s on V_t, (2) pore size distribution curve for the standard sample, and (3) pore size distribution curve for the test sample (From ref. [19]).

Mostly octane or decane is used as measuring liquid for these measurements, because they wet most solid materials almost ideally. Details of the experimental procedures for MSCP are described in Refs. [18,19].

2.3.2. Possibilities of MSCP for the investigation of porous structures

MSCP has several substantial advantages over mercury porosimetry and other porosimetric methods:

(a) *Pore size range*. This method with appropriate standard samples can be used for measurements of pore sizes in the range from 1 to 3×10^5 nm.
(b) *The accuracy* of this method depends primarily on the accuracy of measuring the structure of the standard samples by MMP, which is about 1% of the total pore volume. The error (nonreproducibility) of MSCP is less than 1%.
(c) *Capability to investigate all kinds of materials*. One of the main advantages of MSCP is the possibility for investigation of materials with a low mechanical strength, of frail materials and even of powders.
(d) *Possibility to measure samples at fixed levels of compression and/or temperature*, i.e. under conditions in which they are commonly used in different devices.
(e) *Possibility to use for measurements the same liquid* as that, used in real devices (i.e. leading to the same swelling degree of the sample).
(f) *Possibility of repeated measurements on the same sample*. As MSCP is a nondestructive method and measurements do not change or otherwise influence the sample's structure, this structure can be measured repeatedly at different conditions (e.g. in the case of battery electrodes at different discharge stages).
(g) *Possibility of measuring structures with corrugated pores*. As shown in Refs. [19] MSCP gives the possibility to measure the true pore size function, which is not influenced by pore corrugation. It is possible to measure the statistical distribution of the volume of the trapped (blocked) pores V_{tr} vs. both their radii r_{tr} and the radii of the blocking pores (necks) r_b. For this purpose it is necessary to measure the porograms in two modes: (a) by filling of the pores with liquid, and (b) by evaporating the liquid starting from different degrees of filling.

One of the main drawbacks of MSCP is the long time required for performing measurements. Recently an Automated Standard Porometer described in Refs. [20–22] was developed by Porotech Ltd., Canada which substantially simplifies and accelerates the measurements.

2.3.3. Investigation of wetting and sorption properties of porous materials

One of the most pronounced advantages of MSCP is the possibility to investigate the wetting (hydrophilic/hydrophobic or liophilic/liophobic) properties of porous materials. In Refs. [15,19] it was shown that using different working liquids it is possible to measure the wetting angle of liquids with porous materials. Primarily, MSCP measures the distribution of pore volume vs. the capillary pressure p^c, i.e. vs. the parameter $r^* = r/(\cos\theta)$ (henceforth we call this parameter effective pore radius). For partially hydrophobic materials (for which $\theta > 0$ the porosimetric curves measured with water are shifted towards higher values of r^* in respect to the curves measured with octane which wets most materials almost ideally ($\theta = 0^\circ$). The value of this shift for a certain value of pore volume V_n and of the corresponding pore radius r_n allows to determine the

wetting angle of water for pores with the radius i_n:

$$\cos\ \theta = \frac{r_n}{r^*}. \tag{2.2}$$

For porous materials the wetting angles $\theta(r)$ for pores of different size can be different. In this case an average value of the wetting angle θ^* can be calculated and used.

The capillary pressure can also be represented by the thermodynamic Kelvin equation:

$$p^c == \left(\frac{RT}{V_M}\right) \ln\left(\frac{p_s}{p_o}\right) = \frac{A}{V_M}, \tag{2.3}$$

where V_M is the liquid's molar volume, A is the free binding energy liquid-sample, p_s and p_o are the values of the liquid's vapor pressure in the pore and, respectively, with a plane meniscus. Therefore, measurements of porosimetric curves by MSCP allow to establish not only the dependence of the amount of liquid in the sample on the capillary pressure p^c (isotherm of capillary pressure), but also on the values of parameter p_s/p_o (sorption or desorption) isotherm) and of parameter A (energy isotherm).

For multicomponent porous materials with mixed wettability that are widely used in applied electrochemistry (e.g. fuel cell electrodes containing platinum particles on carbonaceous supports along with different additives) it is possible to investigate separately the structure (pore volume distribution vs. pore size) for hydrophilic and hydrophobic (liophilic and liophobic) pores and to evaluate some important parameters such as the dependence of the fraction of the pore surface occupied by the hydrophobic (liophobic) components on the pore size.

All these advantages and capabilities of MSCP are widely used for investigating different components of fuel cells and processes occurring in fuel cells during their operation.

3. Components of fuel cell electrodes

3.1. The catalytic layer

The catalytic layers of PEM fuel cell electrodes have a complex structure which includes platinum particles deposited on carbonaceous supports, hydrophobic materials (PTFE) and an ionomer (mainly hydrated perfluorosulfonic acid introduced into the layer as a Nafion solution). The hydrophobic additive forms canals for the supply of the reacting gases (hydrogen and oxygen) to the catalyst's surface and for evacuation of the reaction product (water vapor) from the surface. The ionomer provides ionic conductivity within the catalytic layer. Hydrophilic canals (mainly in the carbonaceous support) enable an even distribution of liquid water throughout the catalytic layer. The volume ratio of carbonaceous material and ionomer in the catalytic layers must be chosen so as to attain sufficient high values both for electronic and ionic conductivities. The structural and wetting properties of the carbonaceous support particles influence to a great extent the properties of the catalytic layer and thus the efficiency of the fuel cell. A detailed study of these aspects began only recently.

3.1.1. The porous structure of the catalytic layer

In Ref. [23] the method of standard contact porosimetry (MSCP) was used for investigating an E-TEK catalytic layer with 40% Pt on carbon black of the Vulcan XC-72 type and 5% ionomer (from a Nafion solution in ethanol). This investigation was not systematic enough and did not include other types of catalyst supports.

In Ref. [24] a detailed investigation of the porous structure of ten different carbonaceous support materials was described as well as the modification of this structure during different preparation stages of the catalytic layer, viz. the addition of the Nafion ionomer and the deposition of the platinum catalyst. The use of ten carbonaceous materials with different properties and different values of the specific surface area made it possible to investigate the influence of the support's pore structure on the deposition of the ionomer.

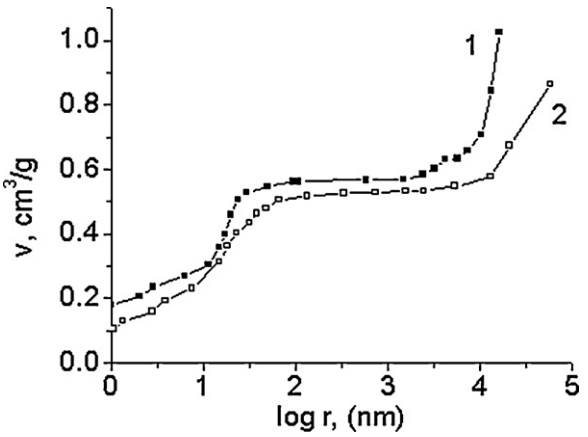

Fig. 2. Integral curves of pore volume distribution vs. pore size V, log r for samples of Sibunit 20P without (1) and with (2) addition of the Nafion ionomer. (From ref. [24]).

It was shown that the pore volume of these materials is formed both by intragranular (primary) mesopores with radii below 10^3 nm (mainly in the range between 0.3 and 50 nm) and by intergranular (secondary) pores with radii larger than 10^3 nm.

Upon addition of the ionomer the total pore volume increases due to the formation of an additional intergranular porous structure. At the same time, the intragranular porosity of the granules decreases. This can be explained by the ionomer blocking the inlets of mesopores without entering into them ("gluing" the pores). This blocking diminishes the internal surface area of mesopores. For different samples of carbonaceous materials different degrees of blocking were observed. Fig. 2 shows integral porosimetric curves for a sample of a Siberian carbon black Sibunit 20P. Curve 1 is for the pure material and curve 2 for the same material after adding 17% of the Nafion ionomer. It can be seen that after addition of the ionomer the volume of pores with radii lower than 10^3 nm substantially decreases. Similar porosimetric curves were recorded for other carbon black samples, viz. for Vulcan XC-72 carbon black, a material most often used in fuel cells as catalyst support. In the case of another (nanofibrous type) carbonaceous material KVU-1 the volume decrease after adding the ionomer is not so distinctly pronounced as for Sibunit 20P and other carbon blacks. No correlation between the degree of blocking and the porous structure could be found. For this reason it was assumed that the degree of blocking depends on the surface properties of the carbonaceous material (nature and amount of surface groups).

3.1.2. The wetting and sorption properties of the catalytic layer

In Ref. [24] results of wetting properties investigations for the same carbonaceous materials as those used in Ref. [24] were reported. These properties were measured prior and after introducing the Nafion ionomer. It was found that hydrophobicity increased for most of the investigated materials after introducing the ionomer. Fig. 3 shows for Vulcan XC-72 the dependence of the wetting angle θ on the pore radius r prior and after introducing the Nafion ionomer. It can be seen that this dependence for the pure material curve (1) is very complex (probably due to the presence of different surface groups in pores of different size). After addition of the ionomer the wetting angle increases indicating a hydrophobizing influence of the additive. An analogous increase of hydrophobicity is also observed for some other carbon blacks. Thus in these materials the ionomer not only provide proton-conducting paths in the catalytic layer, but also acts as a hydrophobizing agent.

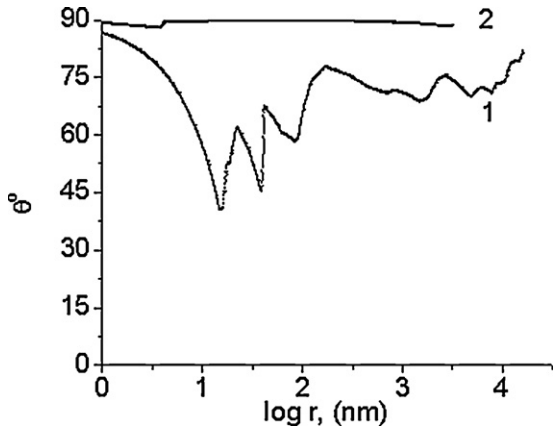

Fig. 3. Dependence of wetting angle θ on effective pore radius r^* for Vulcan XC-72 (1) prior and (2) after introduction of the Nafion ionomer. (From ref. [25]).

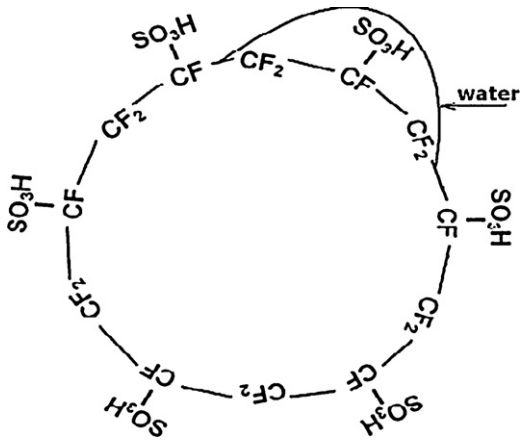

Fig. 5. Schematic of Nafion ionomer particles on carbonaceous materials of the KVU-I type (From ref. [25]).

The hydrophobizing influence of the ionomer can be explained by an orientation of the sulfogroups located on the external surface of the adsorbed ionomer in the direction away from the surface of the carbonaceous material, and the fluorine-containing groups ($-CF_2-CF_2-$) pointing outwards (Fig. 4).

For some other carbonaceous materials the ionomer on the contrary increases the hydrophilic properties. Thus, measurements on KVU-I show that the addition of the ionomer leads to a decrease of the wetting angle. This indicates that on these materials the sulfogroups of the adsorbed ionomer particles have an orientation in the direction opposite than mentioned above (Fig. 5). It seems that the orientation of the sulfogroups of adsorbed ionomer particles depends on the surface properties of the carbonaceous material. The orientation of the sulfogroups is connected with their adhesion energy to the carbon surface that is influenced by the surface properties. Thus, the surface properties of these materials influence both the degree of pore blocking and the wetting properties of the catalytic layers. A detailed knowledge of this influence is important for optimization of the properties of catalytic layers. It was shown in Ref. [25] that the nature and amount of surface groups on carbonaceous materials depend on the preparation process of these materials.

It seems that such an orientation inversion of ionogenic groups with respect to the polymer chain, which was observed in Ref. [24], is characteristic not only of the investigated system. An analogous phenomenon was observed in Ref. [26] for quite different ionogenic groups in phenolsulfocationite membranes of the Polycon-type. This indicates the possibility that such inversions are quite common for ion-exchange resins. This fact is of great importance for the physical chemistry of ionites. This phenomenon can be regarded as a particular case of templating effects described in Refs. [27,28], i.e. of an influence of the support's structure on the properties of very thin deposited layers. When making such a comparison, it must be taken into account that such an inversion of the ionogenic groups occurs only in the surface layer of the ionomer with a thickness of about 1 nm.

Table 1 shows the main integral parameters of the porous structure and wetting properties at different preparation stages of catalytic layers containing the carbonaceous materials Sibunit 20P and KVU-I.

Fig. 6 shows energy isotherms (dependence of water content on the binding energy V, $\log A$) calculated according to Eq. (2.3) for samples at different production stages of the catalytic layer. These isotherms characterize the interaction of water with the composite material. The isotherms were measured in a range including six orders of magnitude of A. With increasing values of A the nature of this interaction changes: from simple filling of smaller and smaller macropores, to capillary condensation of vapor in mesopores, then, in micropores, to a hydration of ionogenic groups and to adsorption. Thus, these isotherms describe in more detail the interaction of water with the catalytic layer components than other kinds of isotherms.

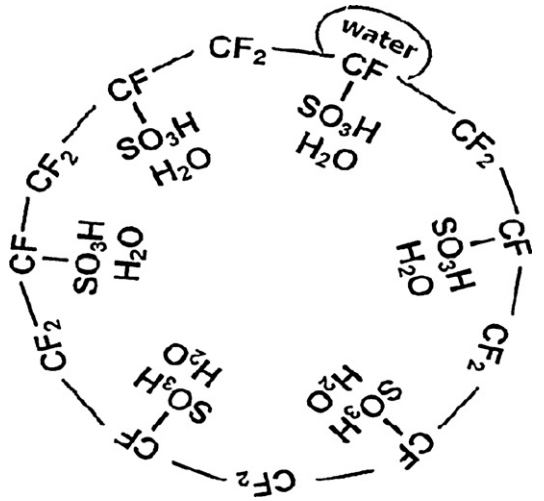

Fig. 4. Schematic of Nafion ionomer particles on carbonaceous materials of the Vulcan XC-72 type. (From ref. [25]).

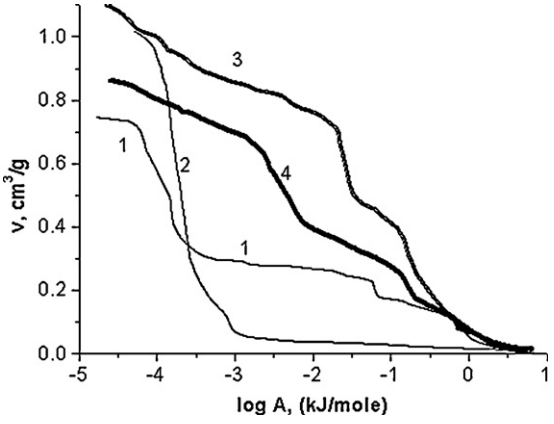

Fig. 6. Integral distribution curves of water content vs. the binding energy of water (V, $\log A$) for the samples: (1) Sibunit 20P, (2) Sibunit 20P + 17% Nafion, (3) Sibunit 20P + 30% Pt, (4) Sibunit 20P + 30% Pt + 17% Nafion (From ref. [25]).

Table 1
Main structural and wetting parameters of catalytic layers with carbon blacks Sibunit 20 P and KVU-I at different preparation stages.

Samples	Sibunit 20P	Sibunit 20P + 17% Nafion	Sibunit 20P +30% Pt	Sibunit 20P +17% +30% Pt Nafion	KVU-I	KVU-I +17% Nafion
υ ($cm^3\ cm^{-3}$)	0.63	0.75	0.77	0.71	0.59	0.74
S ($m^2\ g^{-1}$)	228	332	324	282	95	60
S_{mea} ($m^2\ g^{-1}$)	132	99	101	73	47	38
υ_{phi} ($cm^3\ cm^{-3}$)	0.47	0.65	0.74	0.63	0.56	0.76
S_{phi}/S	0.2	0.09	0.21	0.60	0.60	0.75

3.2. Catalysts used in fuel cells

3.2.1. Platinum catalysts

In Ref. [29] the structure of platinized platinum (Pt/Pt) and platinum black (Adam's platinum) was investigated. The results are shown in Fig. 7. The samples of platinum black were compressed under the pressure of 150 MPa. Measurements of Pt/Pt are connected with difficulties since the deposited Pt layers are very thin and the amount of working liquid in the pores of these layers is too small to be measured by analytical balances. In order to circumvent this difficulty, platinum was deposited on a platinum mesh and a stack of several discs of this mesh was used for measurements. It was found that in these Pt/Pt samples about 50% of the pore volume is accounted for by micropores having radii $r < 1$ nm. The radii of most of the remaining pores were not higher than 3 nm. This circumstance is very important since the size of such micropores is comparable with the thickness d of the electrical double layer and also with the size of many molecules and ions, especially organic. Both these factors influence adsorption and kinetic properties of the deposits, particularly their intrinsic catalytic activity. Such phenomena were described in Ref. [30].

3.2.2. Platinum–PTFE composits

In order to facilitate the transport of reacting gases to the sites on the catalyst's surface certain amounts of hydrophobizing agents, such as PTFE, are added into the catalytic layers of fuel cells. Composits of platinum and PTFE particles are a particular case of multicomponent porous systems with mixed wettability. According to [19], for a bicomponent system containing a hydrophilic component with a water wetting angle θ_1 and a hydrophobic component with a wetting angle θ_2 the average wetting angle can be found as:

$$(\cos\theta)_{av} = (1-\rho)\cos\theta_1 + \rho(\cos\theta_2) > 0, \quad (3.1)$$

where ρ is the fraction of the pore surface occupied by the hydrophobic component. In order to obtain information on the structural and wetting properties of such systems it is necessary to perform porosimetric measurements with some liquids having different wetting angles with PTFE. In Ref. [31] such measurements were described, in which heptane ($\theta_{PTFE} = 24^\circ$), toluol (49°), acetophenone (73°), furfurol (80°), water (108°), and others were used as working liquids. Fig. 8 shows differential distribution functions of the pore volume in terms of pore radii (r) and ρ-values, $\partial^2 V/\partial\rho\,\partial\log r$ for a layer containing 16% PTFE, calculated from the measured porograms. It can be seen that this function has three maxima-two for hydrophilic and one for hydrophobic pores. From these results it can be concluded that the investigated sample contains only two types of pores – completely hydrophilic, located between platinum particles, and completely hydrophobic, located between PTFE particles. No pores with mixed wettability were recorded. No functions of such kind could be found in the literature.

In Refs. [32,33] a macrokinetic theory was described that allows the calculation of polarization curves for hydrophobized electrodes. The main experimental parameter in equations used in this theory is the specific area S_s of the surface dividing two porous aggregates – that of platinum particles and that of PTFE particles. In Ref. [34] a method for measuring this parameter was described. For electrodes containing 4 wt% platinum the value of $S_s = 3 \times 10^4\ cm^2\ cm^{-3}$ was found. Using this value of S_s and some other structural parameters measured by MSCP, the polarization curves for oxygen reduction in 30% KOH solution were calculated. The calculated curves were in satisfactory accordance with the experimental ones. Differential pore size distribution curves of PTFE agglomerates showed that their diameter varies between 0.1 and several tens of μm, the maximal volume being connected with the range between 0.1 and 0.3 μm (the main range for non-agglomerated particles of the used PTFE suspension is between 0.05 and 0.5 μm).

3.2.3. Platinum catalysts deposited on carbon nanotubes

During the last decade many investigations [35–43] revealed an increased catalytic activity of platinum deposited on carbon nanotubes CNT for the reactions of methanol oxidation and oxygen reduction.

In Refs. [44,45] the porous structure and wetting properties of single walled carbon nanotubes (SWCNTs) and the structure and properties of Pt and Pt/Ru deposits on them were investigated by MCSP. The SWCNTs were synthesized by an electric arc method. According to Raman spectroscopy data they had a narrow size distribution (average diameter about 1.5 nm). Because of their high intrinsic hydrophobic properties they were treated with

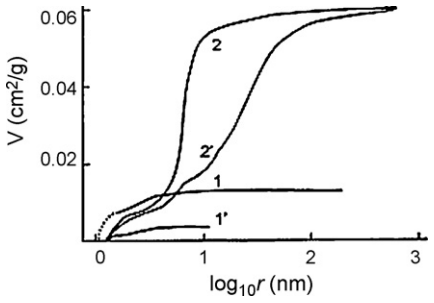

Fig. 7. Integral programs for (1,1') platinized platinum and for (2,2') platinum black (1,2) before and (1',2') after electrochemical sintering (From ref. [30]).

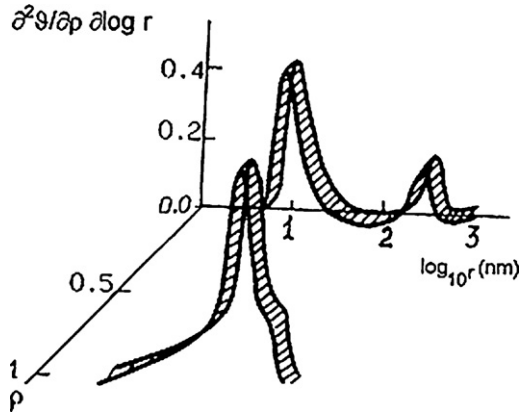

Fig. 8. Differential pore volume distribution vs. pore radii r and vs. hydrophobicity factor ρ for a platinum electrode containing 16% PTFE (From ref. [18]).

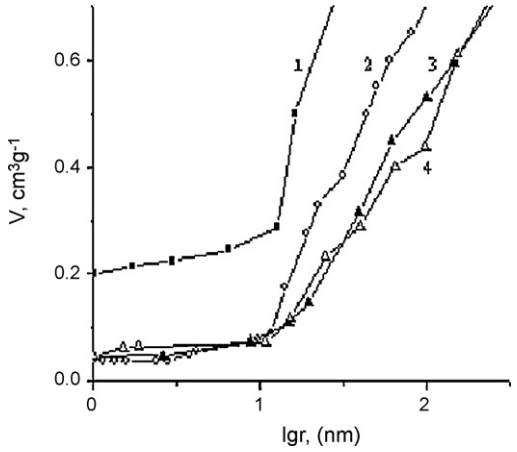

Fig. 9. Integral programs measured with octane (1,3) and water (2,3) for SWCNT (1,2) and $SWCNT_f$ (3,4) (From ref. [46]).

a mixture of sulfuric and nitric acids in order to give them some degree of hydrophilicity (this procedure leads to the formation of hydroxyl and carbonyl surface groups). Fig. 9 shows integral curves of pore volume distribution vs. effective pore radii r^*, measured with octane (1,3) and water (2,4) for the native (1,2) and (3,4) for the treated (functionalized samples denoted as $SWCNT_f$).

In Table 2 the overall and the hydrophilic pore surface areas of the SWCNTs are listed, as well as the true surface area of the Pt/Ru catalyst found by measuring the amount of electric charges needed for oxidation of adsorbed carbon monoxide. The catalyst's specific surface area was found by referring the true surface area to the amount of deposited metals. For comparison data for Vulcan XC-72 carbon black are also shown.

From the data in this table it can be seen that the overall surface area of the treated $SWCNT_f$ measured with octane is substantially lower than that of the native sample mainly as a result of a decline of the micropore volume. It can be assumed that the surface groups inside the treated $SWCNT_f$ block the access of octane into the nanotubes. BET measurements confirm the blocking effect. Furthermore, the surface groups can link adjacent tubes which form aggregates and block parts of the external surface. The hydrophilic surface area of $SWCNT_f$ measured with water is higher than the overall surface area of the native SWCNT, measured with octane. This can be explained by swelling of the nanotubes in water.

Measurements of the catalyst's specific surface area on different supports show that for very small deposit amounts (4–5 $\mu g\,cm^{-2}$) on $SWCNT_f$ high values (250–350 $m^2\,g^{-1}$) of this specific area can be reached. On original SWCNT and on Vulcan XC-72 carbon black these values are much lower. With increasing deposition time the crystallite size increases and the specific area decreases. For a 10 $\mu g\,cm^{-2}$ deposit on $SWCNT_f$ the specific surface remains 2–3 times higher than for other supports. At higher deposit amounts (70–80 $\mu g\,cm^{-2}$) this difference is no longer observed.

In Refs. [44,45] it was found that the specific catalytic activity of deposited platinum catalysts (referred to a unit of the working surface) does not depend on the nature and properties of the support. But it must be noted that on $SWCNT_f$ with 5–10 $\mu g\,cm^{-2}$ of platinum deposits it is possible to achieve values of the working surface up to 300 $m^2\,g^{-1}$ and thus very high overall current densities.

In Ref. [17] the investigation of a step-by-step platinum deposition on a porous titanium support was described. It was shown that during this process the main maximum on the differential porograms shifts towards lower-sized pores. This is due to platinum deposition on the surface of large pores leading to a gradual diminishing of their size.

Table 2
Specific surface area (SPA) of carbonaceous supports and deposited Pt/Ru catalysts.

Support	Overall SPA measured w/octane, $m^2\,g^{-1}$	SPA of mesopores measured w/octane, $m^2\,g^{-1}$	SPA of micropores measured w/octane, $m^2\,g^{-1}$	Overall SPA. of hydrophilic pores, $m^2\,g^{-1}$	SPA of hydrophil. mesopores, $m^2\,g^{-1}$	SPA of hydrophil. micropores, $m^2\,g^{-1}$	SPA share of hydrophilic pores, %%	Amount of deposited Pt/Ru catalyst, $\mu g\,cm^{-2}$	SPA of deposited Pt/Ru catalyst, $m^2\,g^{-1}$
Vulcan XC-72	205	125	80	205	125	80	100	12	49
								40	85
								76	54
								200	45
SWCNT	465	125	340	104	74	30	22	12	85
								27	85
								80	83
								230	61
$SWCNT_f$	100	52	48	121	64	57	1.21	4.1	362
								5.5	255
								6.9	166
								9.7	138
								18	105
								29.5	39
								52	37
								66	76

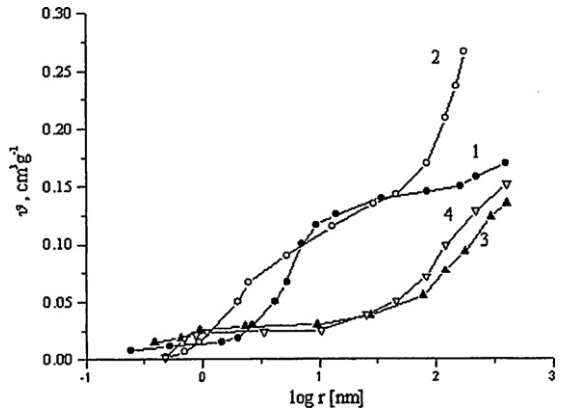

Fig. 10. Integral programs for electrochemically (1,3) and chemically (2,4) synthesized polyaniline measured with water (1,2) and decane (3,4) (From ref. [54]).

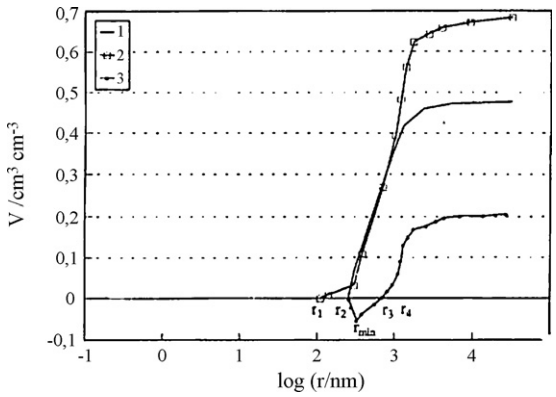

Fig. 11. Integral programs for: (1) an initial SOFC anode, (2) the same anode after removing all nickel particles; curve (3) was calculated by subtracting the volumes in curve (1) from those in curve (2) (From ref. [55]).

3.2.4. Electron-conducting polymers as catalyst support

Some recent publications [46–49] describe the use of electron-conducting polymers (mainly polyaniline) as catalyst supports for the oxidation reactions of methanol, formaldehyde, and formic acid, and mentioned the prospects of using these materials in fuel cells. The porous structure of these polymers influences the distribution of the platinum deposits and hence their properties and catalytic activity.

In Refs. [50–53] the structure of polyaniline (PAni) and polyparaphenylene was investigated. Fig. 10 shows integral porograms for electrochemically and chemically synthesized PAni measured with water and with decane. It can be seen that in water the porosity is much higher than in decane. This increase is due to swelling of the material with the formation of a large amount of new small pores with radii from one to several tens of nm. The degree of swelling of PAni depends on the nature of the counter-ions (i.e. the nature of the emeraldine salts). According to the swelling degree the emeraldine salts can be classified in two groups. The first group includes inorganic salts (with the anions BF_4^-, PO_4^-, Cl^-, HSO_4^-. $HCOO^-$) which are hydrophilic and have a high swelling degree. The second group includes non-swelling hydrophobic salts with $CH_3C_6H_4SO_3^-$ and CF_3COO^- anions. The porograms of the hydrophilic salts show a sharp volume increase in a narrow range of pore sizes of about 100 nm. The PAni salt structure depends to a great extent on the doping degree. Doping the emeraldine base with chloride ions increases the pore volume from 1.0 to 1.7 $cm^3 g^{-1}$ and the specific surface area from 310 to 520 $m^2 g^{-1}$. It was also shown that the structure of the eneraldine base prepared from different precursors (emeraldine chloride, sulfate, and phosphate) differs. This can be regarded as some sort of "memory effect".

Table 3 shows for emeraldine salts the values of the specific pore volumes υ, of the pore surface area S, and of the average radii R_f of single PAni fibrils. From this table it can be seen that for hydrophilic PAni salts the specific surface area is very high – from 400 to 600 $m^2 g^{-1}$. It is situated mainly in the range of micro- and mesopores. These values are of the same order of magnitude as for carbonaceous catalyst supports (see Section 3.1.1).

Summarizing all these results it can be said that the lability of the PAni structure and the presence of nanosized pores (from 1 to 100 nm) favor the formation of nanosized platinum particles, prevent their aggregation and preserve a high surface area of this catalyst. However structures with such a high lability are probably prone to changes and to degradation processes under the influence of external factors.

3.2.5. Catalysts for solid oxide fuel cells (SOFC)

The anodes of solid oxide fuel cells are commonly prepared from a cermet material containing highly dispersed nickel powder and a solid electrolyte ceramic material – mostly yttrium stabilized zirconium (YSZ) that provides sufficient ionic conductivity within the electrode [1,2]. In order to enable transport of the reacting gases to the nickel catalyst's surface sites the anodes contain a system of interconnected pores. The electrochemical reaction of fuel oxidation proceeds at the three-phase boundary S_s between Ni and YSZ pores, and the gas phase. For hydrophilic gas-diffusion electrodes in cells with liquid electrolytes this interphase can be determined from differential porosimetric curves dV/dr, r using an equation of the type of Eq. (1.1). For SOFC anodes this method cannot be used since both the catalyst and the electrolyte are solid phases. In Ref. [54] a variety of MSCP was used for measuring the value of S_s.

Fig. 11 shows porograms and Fig. 12 shows micrographs for an anode with nickel catalyst and an electrolyte $ZrO_2 + 8\% Y_2O_3$. Fig. 13 gives a schematic presentation of the anode's structure. At first the initial sample was investigated, then from this sample nickel particles and aggregates of such particles were removed by dissolving in concentrated nitric acid and after a thorough washing and drying the samples were investigated once again. The curve 1 in Fig. 11 is a porogram for the initial sample and curve 2 was measured after the mentioned procedure. In the range $r < r_2$ curve 2 shows new pores with volume υ_1 that could not be seen in curve 1, due to dissolution of small Ni particles formerly embedded in electrolyte aggregates (position 1 in Fig. 13). These pores do not contact with the gas. Thus, their surface area is not included in S_s. The volumes υ_2 in curve 3 were calculated by subtracting the volumes in curve 2 from those in curve 1. In the range of small pores these volumes are negative, they correspond to pores inside Ni aggregates (position 2 in Fig. 13). These pores do not contact with the electrolyte and therefore are also not included in the value of S_s. The pores which form the surface area S_s have radii $r > r_{min}$ where r_{min} is the radius

Table 3
Structural parameters of emeraldine salts.

	Cl^-	HSO_4^-	$H_2PO_4^-$	BF_4^-	$HCOO^-$	$CH_3C_6H_4SO_3^-$	CF_3COO^-
S ($m^2 g^{-1}$)	590	515	490	470	430	0	0
υ ($cm^3 cm^{-3}$)	0.05	0.45	0.55	0.60	0.40	0.06	0
R_f (nm)	2.10	2.45	2.50	2.70	2.90		

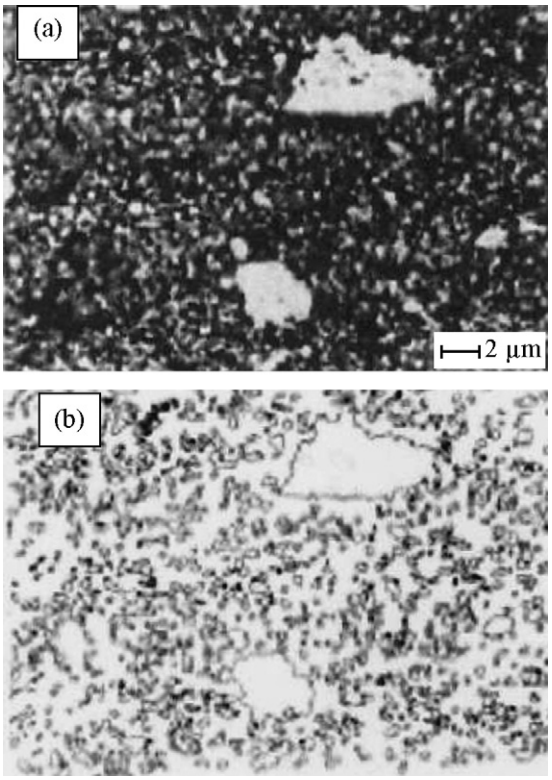

Fig. 12. (a) Micrograph of the initial anode; bright: electrolyte particles, grey: nickel agglomerates, black: pores; (b) micrograph of the same sample after removing nickel (From ref. [55]).

at the minimum of curve 3. The value of S_s can be found from the porogram curve 3 by an expression analogous to Eq. (1.1). The values of S_s for the investigated samples were in the range from 0.98 to 1.24 $m^2\ cm^{-3}$.

In Fig. 12(a) a micrograph for this anode is shown. The white spots represent the electrolyte, the grey ones – nickel particles, and the black ones – the pores. Fig. 12(b) is a micrograph of this anode after removing nickel from the sample. From the micrographs the number N of contacts on the three-phase boundary was evaluated. For different samples (fresh prepared, aged, etc.) this value varied from 1.5×10^6 to 3.4×10^{10}. This value was always proportional to that of S_s and to that of the hydrogen oxidation current density. Thus it can be stated that S_s is the electrochemically active specific surface area. From the curve 2 in Fig. 11 the surface area S_{Ni} of all nickel particles was found. This value is much higher than that of S_s.

Fig. 13. Schematic representation of the anode structure (From ref. [55]).

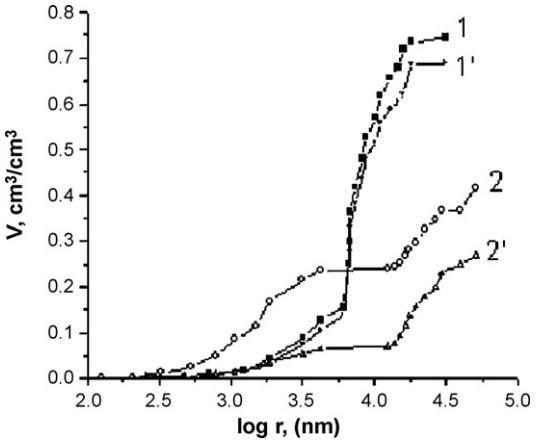

Fig. 14. Integral distribution curves V, log r^* measured with octane (curves 1, 1') and with water (curves 2,2') for the pure Toray carbonaceous paper and (curves 1,2,) and for the paper containing 27 w% PTFE (1',2') (From ref. [58]).

It follows from these data that the value of S_{Ni} has no influence on the anode performance. The values of S_s can be used for evaluating the kinetics of hydrogen oxidation.

3.3. The gas-diffusion layer (GDL)

The porous structure and balance of wetting properties of the pores influence transport processes in GDLs and as a consequence the efficiency of fuel cells. A comprehensive review on gas-diffusion layers for PEMFCs was recently published by Cindrella et al. [55]. This review discusses in details the role of the GDL structure and wetting properties on gas and liquid transport processes within the layer. However up to now, due to lack of appropriate methods, these properties of GDLs were not investigated in detail and only few publications devoted to a quantitative assessment of parameters of these properties can be found in the literature.

In 2006 Gurau et al. [56] investigated the average values of the internal wetting angles for different GDL samples by combining the Washburn method mentioned in part 2 (involving water as test liquid) with measurements involving other liquids (hexane, toluene, acetone, methanol, etc.).

Investigations by MSCP of GDLs on the base of carbonaceous Toray paper were described in Refs. [57,58]. Fig. 14 shows integral distribution curves V, log r^* measured with octane and water for the pure carbonaceous paper and for the paper containing 27 wt% PTFE. The curves measured with octane show that the paper in its initial state had a highly monodisperse porous structure mainly with pore radii from 10 to 30 μm and with an overall porosity of about 75%. After treatment with a PTFE suspension a certain decrease in the overall porosity can be observed. Due to the poorer wettability of carbon with water a shift of curves 2 to higher r^* values could be expected. It can be seen that this is the case only for the paper containing PTFE. For the pure paper a well-pronounced volume increase in the region of smallest pores ($r < 0.6$ μm) can be observed. This is due to a swelling influence of water on the fibers in the region of small pores (with high surface area). In the presence

Table 4
Porosity of Toray paper with different amounts of PTFE.

Porosity, $cm^3\ cm^{-3}$	c_{PTFE} (wt%)		
	0	18	27
υ	0.75	0.70	0.69
υ_{hi}	0.42	0.29	0.27
υ_{pho}	0.33	0.41	0.42
ξ		2.3	1.6

of PTFE the sorption of water and the swelling degree are obviously decreased.

Table 4 shows the porosities (pore volume per unit of sample volume) for hydrophilic pores υ_{phi}, hydrophobic pores υ_{pho}, and the overall porosity $\upsilon = \upsilon_{phi} + \upsilon_{pho}$ for Toray paper with two values of PTFE concentrations c_{PTFE}. In Ref. [58] the notion of hydrophobizing efficiency ξ was introduced which represents the ratio of hydrophobic pores (in volume percents) to the PTFE concentration (in volume percents or, as carbon and PTFE have similar density values, in weight percents). This parameter is of importance since high values of the PTFE concentration can lead to an increase of the GDL's ohmic resistance. From the table it can be seen that the PTFE concentration does not significantly influence the volumes of both hydrophilic and hydrophobic pores. At the same time, at the higher concentration the hydrophobizing efficiency significantly declines. This is probably due to the fact that at higher concentration PTFE particles are deposited mainly at the surface of previously deposited particles, not on the carbon surface and thus do not substantially increase the hydrophobic properties.

An investigation of water wetting angles for Toray paper containing 27% of two different hydrophobizing agents: suspensions of F-4D $(-CF_2-CF_2-)_n$ and of FEP 121A $(-CF_2-CF(CF_3)-CF_2-)_n$ showed that the average value of the wetting angle θ^* was 65° for F-4D and 78° for FEP121A. For samples containing FEP121A the efficiency was $\xi = 3.4$, i.e. significantly higher than that for samples containing F-4D. Thus FEP121A containing highly hydrophobic CF_3 groups has a much stronger hydrophobizing influence on the GDL than F-4D.

4. Membranes

Different types of membranes: porous inorganic capillary membranes soaked with electrolyte solutions or polymeric ion-exchange membranes are one of the most important components of fuel cells [1,2]. Membranes are also used in other fields of applied electrochemistry such as electrolysis and electrodialysis.

MSCP is extremely well suited for investigations of membrane structures since it is possible not only to use the same working liquid as in real fuel cells (resulting in the same swelling degree), but also the same compression degree as that used in fuel cell stacks.

4.1. Capillary membranes

The structure of chrysotile asbestos, which is widely used as separator in different electrochemical devices (alkaline fuel cells, electrolysers, etc.), was studied in Ref. [19]. As working liquids octane, water, and a solution of 7 M KOH were used. For alkaline (or other electrolyte) solutions the method of changing the overall amount of liquid in the samples by its evaporation cannot be used,

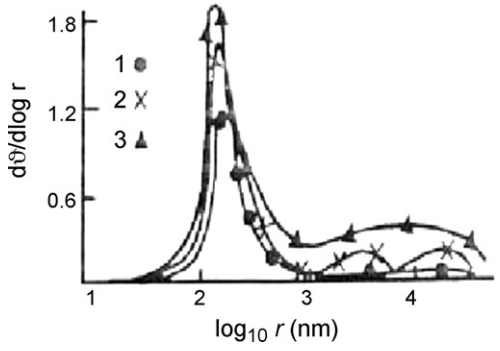

Fig. 15. Differential porograms for asbestos measured with different working liquids: (1) octane, (2) water and (3) solution of 7 M KOH (From ref. [19]).

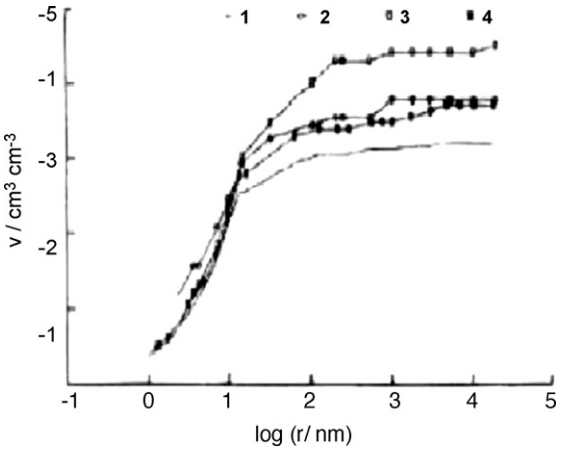

Fig. 16. Integral porograms for membranes: MF-4SK (1), Nafion 112 (2), Nafion 115 (3), and Nafion 117 (4) (From ref. [60]).

since during water evaporation or condensation the solution concentration changes. A modified method was developed in which the amount of liquid in the porous bodies is changed by capillary soaking or drying. In the first case the dried test sample is brought into contact with several standard samples, filled with different amounts of liquid. In the second case the completely filled test sample is contacted with dried standard samples. In Fig. 15 differential porograms obtained by this method are shown. In octane (curve 1) there is practically no swelling of asbestos and the porogram is characteristic for its native porous structure. In water (curve 2) swelling is due to an increase of the volume of macropores with radii in the range from 1×10^3 to 4.5×10^4 nm. In the alkaline solution (curve 3) there is a further volume increase in the range of the largest pores. It must be noted that the formation of large pores in alkaline solutions can have serious consequences, viz. a mixing of reacting gases in the case of insufficient amount of liquid in the MEA.

4.2. Homogeneous ion-exchange membranes

Ion-exchange membranes most widely used in fuel cells of the PEMFC and DMFC type are perfluorosulfonic acid (PFSA) membranes of the Nafion® type. Several versions of such membranes are known. The structure of the membranes Nafion 112, Nafion 115, Nafion117 (DuPont, USA) and the Russian-made version MF-4SK was investigated in Ref. [59] using water as working liquid. From the integral porograms shown in Fig. 16 it can be seen that the main part of pore volume is connected with micro- and mesopores with radii $r < 10$ nm (henceforth, this range is called nanostructure). In this range there is no substantial difference between the curves for different versions of the membrane. It can be assumed that this nanostructure depends mainly on the chemical nature of the membrane. In the range of larger pores with $r > 500$ nm the curves diverge. It seems that these large pores are formed due to technological factors, leading to a certain degree of surface roughness. This assumption is corroborated by optical investigations. Measurements with octane and with water showed that these surface pores of the membranes are hydrophobic. This can be only explained by a model, according to which the sulfogroups on the membrane surface have an orientation vs. the inside of the membrane. This agrees with the results of wetting angle measurements for water drops in the presence of water vapor, reported in Ref. [60] and also with the phenomenon of ionogenic group's orientation inversion with respect to the polymer chain, described in Section 3.1.1.

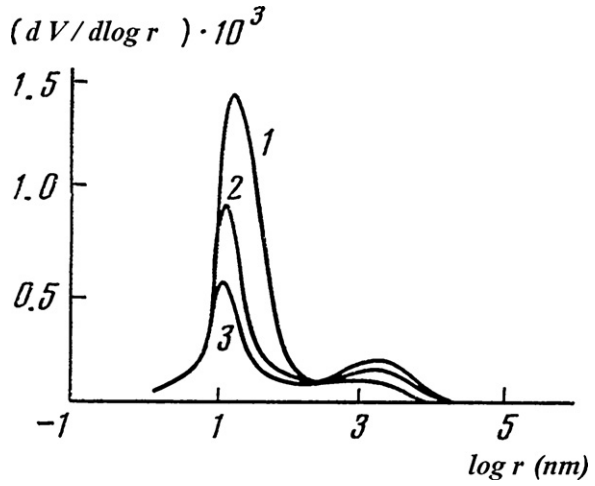

Fig. 17. Differential porogramms for the heterogeneous membrane MK-40. DVB content: (1) 2%, (2) 4%, (3) 8% (From ref. [63]).

In Ref. [61] it was shown that any changes in the preparation method have an influence on the porous structure, for example an increase in the ion-exchange capacity of membranes MF-4SK from 0.71 to 1.02 mg-equiv. g^{-1} leads to an almost twofold porosity increase in water.

The swelling of MF-4SK membranes in different liquids was studied in Ref. [61]. It was shown that the nature of the liquid has a significant influence on the porous structure of the swollen membrane. The overall volume of the nanostructure pores in ethanol is almost twice as high as in water. This observation is of importance with respect to direct ethanol fuel cells. The swelling of ion-exchange membranes depends on the nature of the counterions. In membranes MF-4SK the substitution of protons by Na^+ ions lowers the porosity for about 30%. The membranes pore volume significantly decreases upon transition from inorganic to organic counter-anions.

4.3. Heterogeneous ion-exchange membranes

Heterogeneous membranes contain other components in addition to the ionite. The heterogeneous cationite membrane MK-40 which is prepared by co-polymerization of styrene and divinylbenzene (DVB) was investigated in Ref. [62]. As binding agents in these membranes polyethylene particles are used. On the differential porograms shown in Fig. 17 two maxima can be seen, one in the range of micro- and mesopores with radii from 1 nm up to about 100 nm, the other in the range of macropores with radii 300–3000 nm. The pores of the first type are formed as a result of swelling of the ionite phase and the pores of the second type are formed by the inert polyethylene particles. The mesopores are probably formed between fragments of polyethylene and DVB. Thus, from the ratio of the sum of micro- and mesopore volumes to the overall pore volume the homogeneity degree of membranes can be evaluated.

4.4. Composite membranes

Polymeric fibrous composites are a new type of ion-exchange membranes. A combination of materials with a fibrous structure and those with ion-exchange properties allows to manufacture new membranes with a broad range of predetermined properties. The structural and wetting properties of such a composite membrane "Polycon" were investigated in Ref. [26]. This membrane is produced by casting a phenolsulfocationite monomer on a fibrous PAni matrix and a subsequent pressure application, during which exothermic heat is developed. In a swollen state the structure of this membrane is a combination of the fibrous matrix structure and the structure of the swollen ionite. The matrix contains hydrophilic micropores, mesopores with mixed wettability, and a small amount of hydrophobic meso- and macropores. It was found that for samples of this material produced under different conditions the surface area of the ionite pores varies from 70 to 480 $m^2\ g^{-1}$. This, again, can be explained by a different orientation of the ionogenic groups with respect to the polymer chain.

In Ref. [63], the structure of a membrane used for phosphoric acid fuel cells (PAFC) was investigated. This membrane was prepared by pressing and sintering silicium carbide and PFTE powders. Hydrophilic pores account for about 90% of the overall pore volume. The size of these pores varies from 0.1 to 80 μm; the main pore volume being connected with pores of size 10–50 μm.

4.5. Pore corrugation in membranes

In Section 2 of this review it was mentioned that MSCP allows to investigate pore corrugations. In Ref. [64] such investigations were described for the homogenous membrane MA-100 and also for self-made heterogeneous membranes with carboxylic groups which were prepared by co-polymerization of methacrylic acid and DVB in a polyethylene solution acting as a binding agent. For these investigations the integral pore size distribution was measured by MSCP for the dry membranes during octane desorption and for the swollen membranes during water adsorption and desorption. For the homogenous membranes a considerable (up to ninefold) volume increase in the nanostructure range was observed in water. In the macrostructure range there was practically no volume change in comparison with the dry membrane.

The most important result of these measurements is the coincidence of the adsorption and desorption curves for the swollen homogeneous membranes in the nanostructure range and a slight hysteresis in the macrostructure range. For the heterogeneous membrane, also, a complete coincidence of the curves in the nanostructure range was observed, whereas the hysteresis in the macropore range substantially increased. It follows from these results that the nanostructure pores that are formed during swelling are not corrugated whereas the macropores show a high degree of corrugation. Taking into account that pore corrugation leads to a decrease of the ionic conductivity this result can be regarded as one of the possible explanations for the high conductivity of the homogenous Nafion membranes.

4.6. Influence of compression and temperature on the porous structure

In fuel cell batteries the membranes are compressed during compression of the whole fuel cell stack. In Ref. [64] the influence of the applied pressure on the pore structure was investigated. With increasing pressure the volume of large pores decreases. The smallest pore size, for which this decrease can be observed, decreases with increasing pressure, i.e. small pores are less prone to deformation by pressure.

In Ref. [59] the influence of temperature on the porous structure of Nafion 117 membranes was investigated. It was shown that a temperature increase from room temperature (20 °C) to the working temperature of PEMFCs (80°C) leads to a reduced porosity in the range of pores larger than 10 nm.

4.7. Isotherms of capillary pressure and water desorption

In Ref. [59] measurements of capillary pressure isotherms for different types of Nafion membranes were described. Fig. 18 represents such isotherms for Nafion 117 at temperatures of 20 and 80 °C.

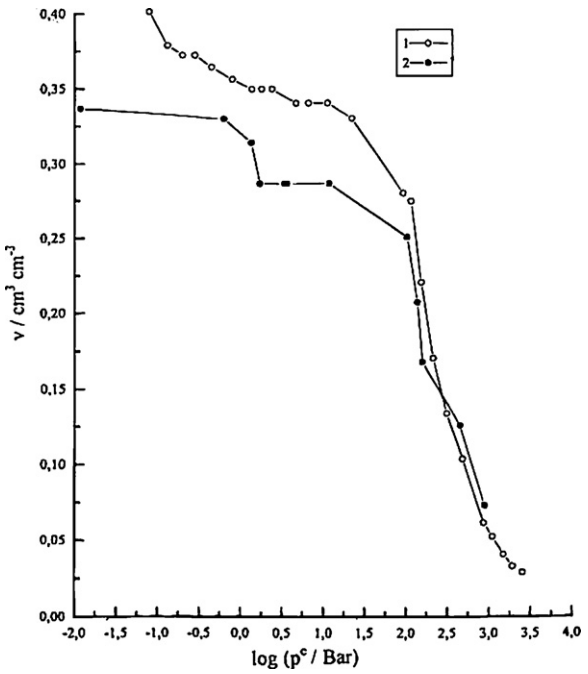

Fig. 18. Isotherms of capillary pressure for the Nafion 117 membrane at temperatures: (1) 20 °C, (2) 80 °C (From ref. [60]).

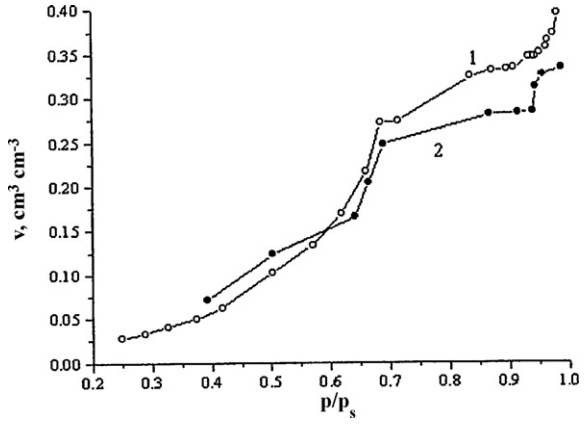

Fig. 19. Isotherms of water desorption for the Nafion 117 membrane at temperatures: (1) 20 °C, (2) 80 °C (From ref. [60]).

A theoretical analysis of processes of water management in PEMFCs reported in Ref. [65] shows that capillary pressure isotherms are of great importance for optimization of these processes. In particular, high values of p^c prevent an excessive drying of the membrane near the anode at high current densities and thus improve fuel cell's discharge possibilities.

Fig. 19 shows isotherms of water desorption, i.e. the dependence of water content V on the values of p_s/p_o calculated according to Eq. (2.3) for Nafion 117 membranes at temperatures of 20 and 80 °C. These isotherms are of importance since, depending on mass-transport processes, the relative humidity in the gas chambers adjacent to the membranes can vary substantially. The corresponding changes in the membrane's water content influence the conductivity of the membrane and, hence, the fuel cell performance. From the figure it can be seen that a lowering of the p_s/p_o value from 1.0 to 0.8 at 80 °C leads to a 20% decrease of the membrane's water content, that can substantially lower the performance of PEMFCs.

5. The membrane-electrode assemblies

In Ref. [66] the influence of flooding conditions of individual fuel cell components on efficiency and main electrical and operational parameters of fuel cells was analyzed. The membrane-electrode assemblies (MEAs) consist of several porous components (GDLs, catalytic layers of both electrodes and the membrane). All these components are soaked with liquids. In the case of PEMFCs and DMFCs these liquids are water or aqueous methanol solutions. For PAFCs, alkaline fuel cells, and MCFCs these liquids are phosphoric acid or alkaline solutions. or, respectively, carbonate melts. Each of the porous components has its own structural, wetting, and other properties.

As shown above, MSCP allows measuring for each porous component j the isotherm of capillary pressures:

$$\upsilon_j = f(p^c), \tag{5.1}$$

where υ_j is the volume of liquid in this component (flooding degree).

The overall volume of the liquid in the MEA $V = \Sigma\upsilon$ depends on the initial volume V_o and, in the case of water and aqueous solutions, on the external conditions of water removal. In the MEA all porous components are in close contact and, thus, the liquid in all of them is in a state of thermodynamic capillary equilibrium. This implies that the values of the capillary pressure $p^c{}_j$ are equalized in all porous components. The common value of $p^c{}_j$ corresponds according to Eq. (5.1) to the values of υ_j in the individual components. Therefore, these values depend on the overall flooding degree V:

$$p^c = f(V) \tag{5.2}$$

During discharge of the fuel cell (current flow) the voltage losses due to each component η_j depend on its flooding degree:

$$\eta_j = f(\upsilon_j). \tag{5.3}$$

For instance, lowering of the membrane's flooding degree ("drying of the membrane") leads to a decrease in its conductivity and, thus, to an increase of ohmic voltage losses. An increase in the flooding degree of the catalytic layers hampers access of the reacting gases to the catalyst and, thus, increases losses due to concentration polarization.

One of the parameters that describe the electrochemical efficiency of a fuel cell is the cell's operational voltage U at a given discharge current density. This voltage can be represented as:

$$U = U_0 - \sum \eta_j, \tag{5.4}$$

where U_0 is the open-circuit voltage. Taking into account Eqs. (5.1)–(5.3) we have:

$$U = U_0 - \sum \eta_j = U_0 - \sum f(\upsilon_j) = U_0 - F(V). \tag{5.5}$$

This "flooding equation" describes the dependence of the fuel cell voltage on the cell's overall flooding degree.

A very important problem in the design of fuel cells is that of the compatibility of the different porous MEA components. For instance, when the wetting and/or structural properties of the anode and cathode catalytic layers substantially differ there exists a possibility that one of these layers has a very low and the other layer a very high flooding degree. In this case even if the intrinsic catalytic activity of the layers is very high, the cell voltage will be low as a result of gas transportation limitations in the second of these layers. Incompatibility of the membrane and the catalytic layers exists also when in the flooding range (the overall value V of the liquid) where the polarization of the catalytic layers is minimal the flooding degree of the membrane is low. In this case not only

the ohmic losses in the membrane increase, but a mixing of the reacting gases (oxygen and hydrogen) through dry pores is possible leading to a detonation danger. One of the functions of GDLs or special additional porous buffering layers is to minimize possible changes of the flooding degree of other thin components. For this reason the thickness of GDLs is often higher than that of other layers.

In Ref. [67] a graphical method was described that allows the assessment of the flooding degree changes of different MEA components during changes of the overall value V.

6. Conclusion

It follows from the above, that the distribution of the liquid's volumes among the MEA's porous components is of prime importance for the fuel cell's electrical and operational parameters. For modelling processes in fuel cells and for optimizing these processes a detailed knowledge of the structural and wetting properties of all porous MEA components is necessary. As a result of structure optimization it is possible not only to improve the electrical parameters (cell voltage at a given discharge current), but also to improve the stability of these parameters under conditions of changing flooding degrees (as a result of frequent changes of discharge current, temperature and/or conditions of water removal).

Bipolar plates are an essential component of most types of fuel cells; they divide adjacent cells in a fuel cell stack. Problems connected with these plates are discussed in a great number of papers and reviews. One of the most important requirements for bipolar plates is a complete absence of gas permeability, i.e. the complete absence of interconnected through-pores, penetrating the plates. The wettability of the plate's channels is of importance for fuel cell performance since accumulation of liquid water in them can hamper the gas supply to the GDLs. However, in the literature no detailed investigations on the wettability of bipolar plates can be found. For these reasons bipolar plates are not covered in this review.

References

[1] W. Vielstich, A. Lamm, H.A. Gasteiger (Eds.), Handbook of Fuel Cells. Fundamentals Technology and Applications, vols.1–4, John Wiley and Sons, Ltd, Chichester, England, 2003.
[2] V.S. Bagotsky, Fuel Cells: Problems and Solutions, Wiley, Hoboken, NJ, 2009, 320 pp.
[3] C. Drake, Ind. Eng. Chem. 1 (1949) 780.
[4] M.M. Dubinin, G.M. Plavnik, Carbon 6 (1968) 183.
[5] S. Miklos, A. Pohl, Bergakademie 22 (1970) 97.
[6] M.J. Swata, I. Jansta, Czech. Chem. Commun. 30 (1965) 2455.
[7] S.J. Gregg, K.S.W. Sing, Adsorption, Surface Area and Porosity, Academic Press, NY, 1967.
[8] R.I. Coalson, W.G. Grit, US Patent 3,684,747 (1972).
[9] D.M. Bernardi, M.V. Verbrugge, J. Electrochem. Soc. 139 (1992) 2477; J. Electrochem. Soc. 234 (1978) 125.
[10] D.S. Watkins, in: L.M.J. Blomen, M.N. Mugerva (Eds.), Fuel Cell Systems, Plenum Press, NY, 1993, p. 493.
[11] R. Schlögl, H. Schuring, Z. Elektrochem. 10 (1961) 863.
[12] P. Dietz, P.K. Hansma, O. Inacker, J. Membr. Sci. 65 (1992) 101.
[13] E.W. Washburn, Phys. Rev. 18 (1921) 273.
[14] Yu.M. Volfkovich, Dokl. Akad. Nauk SSSR 234 (1978) 125.
[15] Yu.M. Volfkovich, E.I. Shkolnikov, Zh. Phys. Khim. 52 (1978) 210.
[16] Yu.M. Volfkovich, E.I. Shkolnikov, Sov. Electrochem. 15 (1979) 8.
[17] Yu.M. Volfkovich, V.S. Bagotsky, V.E. Sosenkin, E.I. Shkolnikov, Sov. Electrochem. 16 (1980) 125.
[18] Yu.M. Volfkovich, V.S. Bagotsky, J. Power Sources 48 (1994) 327.
[19] Yu.M. Volfkovich, V.S. Bagotsky, Colloid Surf. A: Physocochem. Eng. Aspects 187/388 (2001) 349.
[20] Yu.M. Volfkovich, I.A. Blinov, V.V. Kulbachevsky, V.E. Sosenkin, Porosimeter, US Patent 6,298,711 (2001).
[21] Yu.M. Volfkovich, I.A. Blinov, A. Sakar, Porosimetric Device, US Patent 7,059,175 (2006).
[22] Web-site: www.porotech.net.
[23] Baturina, Y.M. Volfkovich, A.V. Sakars, K.J. Wynne, G.E. Wnek, 207th Meeting of the Electrochemical Society, Quebec, Canada, May 15–20, 2005, Meeting Abstracts.
[24] Yu.M. Volfkovich, V.E. Sosenkin, N.F. Nikolskaya, Russ. Electrochem 46 (2010) 352.
[25] M.R. Tarasevich, Electrochemistry of Carbonaceous Materials (in Russian), Nauka, Moscow, 1984.
[26] Yu.M. Volfkovich, N.A. Kononenko, M.A. Cherniaeva, M.M. Kardash, A.I. Shkabara, A.V. Pavlov, Membranes 39 (2008) 8 (in Russian).
[27] K.S. Napolskii, P.J. Barczuk, S.Yu. Vassiliev, et al., Electrochim. Acta 52 (2007) 7910.
[28] T. Kyotani, W.H. Xu, Y. Yokoyama, et al., J. Membr. Sci. 196 (2002) 231.
[29] T.D. Gladysheva, E.I. Shkolnikov, Yu.M. Volfkovich, B.I. Podlovchenko, Sov. Electrochem. 18 (1982) 337.
[30] B.I. Podlovchenko, T.D. Gladysheva, O.V. Vyaznikovskaya, Yu.M. Volfkovich, Sov. Electrochem. 19 (1993) 424.
[31] Yu.M. Volfkovich, E.I. Shkolnikov, Sov. Electrochem. 19 (1983) 586.
[32] Yu.M. Volfkovich, E.I. Shkolnikov, Sov. Electrochem. 15 (1979) 5.
[33] Yu.M. Volfkovich, E.I. Shkolnikov, Sov. Electrochem. 19 (1983) 1177.
[34] Yu.M. Volfkovich, E.I. Shkolnikov, V.S. Dubasova, V.A. Ponomarev, Sov. Electrochem. 19 (1983) 765.
[35] G. Wu, Y.-Sh. Chen, B.-Q. Xu, Electrochem. Commun. 7 (2005) 1237.
[36] E. Frackowiak, G. Lot, T. Cacciaguerra, F. Beguin, Electrochem. Commun. 8 (2006) 129.
[37] X. Li, I.-M. Hsing, Electrochim. Acta 51 (2006) 5250.
[38] D.-J. Guo, H.-L. Li, J. Power Sources 160 (2006) 44.
[39] C.-H. Wang, H.-C. Shih, Y.-T. Tsai, H.-Y. Du, L.-C. Chen, K.-H. Chen, Electrochim. Acta 52 (2006) 1612.
[40] J. Prabhuram, T.S. Zhao, Z.X. Liang, R. Chen, Electrochim. Acta 52 (2007) 2649.
[41] C.-C. Chen, C.-F. Chen, C.-M. Chen, F.-T. Chuang, Electrochem. Commun. 9 (2007) 159.
[42] M.-C. Tsai, T.-K. Yeh, C.-H. Tsai, Electrochem. Commun. 8 (2006) 1445.
[43] H.J. Wang, H. Yu, F. Peng, P. Lv, Electrochem. Commun. 8 (2006) 499.
[44] E.K. Tusseva, N.A. Mayorova, V.E. Sosenkin, et al., Russ. Electrochem. 44 (2008) 884.
[45] N.A. Mayorova, E.K. Tusseva, V.E. Sosenkin, et al., Russ. Electrochem. 45 (2009) 1089.
[46] G. Wu, L. Li, J.-H. Li, B.-Q. Xu, J. Power Sources 155 (2006) 118.
[47] P. Santosh, A. Gopalan, K.-P. Lee, J. Catal. 234 (2006) 177.
[48] C. Jiang, X. Lin, J. Power Sources 164 (2007) 49.
[49] Z.A. Hu, L.J. Ren, X.J. Feng, et al., Electrochem. Commun. 9 (2007) 97.
[50] Yu.M. Volfkovich, V.S. Bagosky, T.K. Zolotova, E.Yu. Pisarevskaya, Electrochim. Acta 48 (1996) 1905.
[51] Yu.M. Volfkovich, M.D. Levi, T.K. Zolotova, E.Yu. Pisarevskaya, Polym. Commun. 34 (1993) 2443.
[52] Yu.M. Volfkovich, T.K. Zolotova, M.D. Levi, Ya.A. Letuchy, Adv. Mater. 5 (1993) 274.
[53] Yu.M. Volfkovich, A.G. Sergeev, T.K. Zolotova, et al., Electrochim. Acta 44 (1999) 1543.
[54] J. Divisek, R. Wilkenhöner, Yu.M. Volfkovich, J. Appl. Electrochem. 29 (1999) 153.
[55] L. Cindrella, A.M. Kannan, J.F. Lin, K. Saminathan, Y. Ho, C.W. Lin, J. Wertz, J. Power Sources 194 (2009) 146.
[56] V Gurau, M.J. Bluemle, E.S. De Castro, Y.M. Tsou, J. Adin Mann Jr., T.A. Zawodzinski Jr., J. Power Sources 160 (2006) 1156.
[57] Yu.M. Volfkovich, V.E. Sosenkin, N.F. Nikolskaya, T.L. Kulova, Russ. Electrochem. 44 (2008) 1.
[58] .T. Gostik, M.W. Fowler, M.A. Ioannidis, M.D. Pritzker, Yu.M. Volfkovich, A.V. Sakars, J. Power Sources 156 (2006) 375.
[59] J. Divisek, M. Eikerling, V.M. Mazin, H. Schmitz, U. Stimming, Yu.M. Volfkovich, J. Electrochem. Soc. 145 (1998) 2677.
[60] S. Gottesfeld, T.A. Zawodzinski, in: R.C. Alkire, H. Gerischer, D.M. Kolb, C.W. Tobias (Eds.), Advances in Electrochemical Science and Engineering, vol. 5, Wiley–VCH, Weinheim, Germany, 1997, p. 195.
[61] Yu.M. Volfkovich, N.A. Dreiman, O.N. Belyaeva, I.A. Blinov, Sov. Electrochem. 24 (1988) 324.
[62] N.P. Berezina, Yu.M. Volfkovich, N.A. Kononenko, I.A. Blinov, Sov. Electrochem. 23 (1987) 912.
[63] M.A. Khrizolitova, Yu.M. Volfkovich, G.M. Mikhaleva, L.S. Tabakman, Sov. Electrochem. 24 (1988) 709.
[64] Yu.M. Volfkovich, V.K. Luzhin, A.N. Vanyulin, E.I. Shkolnikov, I.A. Blinov, Sov. Electrochem. 20 (1984) 613.
[65] M. Eikerling, Yu.I. Kharkats, A.A. Kornyshev, Yu.M. Volfkovich, J. Electrochem. Soc. 145 (1998) 2684.
[66] Yu.M. Volfkovich, Sov. Electrochem. 14 (1978) 460.
[67] Yu.M. Volfkovich, Sov. Electrochem. 14 (1978) 1282.